HHS Public Access

Author manuscript

Stem Cells. Author manuscript; available in PMC 2018 May 01.

Published in final edited form as:

Stem Cells. 2017 May ; 35(5): 1246–1258. doi:10.1002/stem.2578.

Intravenously Transplanted Human Bone Marrow Endothelial Progenitor Cells Engraft Within Brain Capillaries, Preserve Mitochondrial Morphology, and Display Pinocytotic Activity Towards BBB Repair in Ischemic Stroke Rats

Svitlana Garbuzova-Davis[1,2,3,4,*], **Edward Haller**[5], **Roger Lin**[1], and **Cesario V. Borlongan**[1,2,*]

[1]Center of Excellence for Aging & Brain Repair, Morsani College of Medicine, University of South Florida, Tampa, Florida 33612, United States of America

[2]Department of Neurosurgery and Brain Repair, Morsani College of Medicine, University of South Florida, Tampa, Florida 33612, United States of America

[3]Department of Molecular Pharmacology and Physiology, Morsani College of Medicine, University of South Florida, Tampa, Florida 33612, United States of America

[4]Department of Pathology and Cell Biology, Morsani College of Medicine, University of South Florida, Tampa, Florida 33612, United States of America

[5]Department of Integrative Biology, University of South Florida, Tampa, Florida 33620, United States of America

Abstract

Stroke is a life threatening disease with limited therapeutic options. Cell therapy has emerged as an experimental stroke treatment. Blood-brain barrier (BBB) impairment is a key pathological manifestation of ischemic stroke, and barrier repair is an innovative target for neurorestoration in stroke. Here, we evaluated via electron microscopy the ability of transplanted human bone marrow endothelial progenitor cells (hBMEPCs) to repair the BBB in adult Sprague-Dawley rats subjected to transient middle cerebral artery occlusion (tMCAO). β-galactosidase pre-labeled hBMEPCs were intravenously transplanted 48 hours post-tMCAO. Ultrastructural analysis of microvessels in non-transplant stroke rats revealed typical BBB pathology. At 5 days post-transplantation with hBMEPCs, stroke rats displayed widespread vascular repair in bilateral striatum and motor cortex, characterized by robust cell engraftment within capillaries. hBMEPC transplanted stroke rats exhibited near normal morphology of endothelial cells, pericytes, and astrocytes, without detectable perivascular edema. Near normal morphology of mitochondria was also detected in endothelial cells and perivascular astrocytes from transplanted stroke rats. Equally notable, we

[*]Authors for correspondence: Svitlana Garbuzova-Davis, Ph.D., D.Sc., Cesario V. Borlongan, Ph.D., Center of Excellence for Aging and Brain Repair, Department of Neurosurgery and Brain Repair, Morsani College of Medicine, University of South Florida, 12901 Bruce B. Downs Blvd., Tampa, FL 33612, United States of America, Tel: 813-974-3189 or 813-974-3988, sgarbuzo@health.usf.edu or cborlong@health.usf.edu.

Author contributions: SGD and CVB designed the study; EH performed TEM; RL performed *in vitro* EPC isolation, culture, and characterization; SGD, EH, and CVB performed the data analysis; SGD and CVB wrote the manuscript.

Declaration of conflicting interests

The author(s) declare no potential conflicts of interest with respect to the research, authorship, and/or publication of this article.

observed numerous pinocytic vesicles within engrafted cells. Robust engraftment and intricate functionality of transplanted hBMEPCs likely abrogated stroke-altered vasculature. Preserving mitochondria and augmenting pinocytosis in cell-based therapeutics represent a new neurorestorative mechanism in BBB repair for stroke.

Keywords

MCAO; rats; hBMEPC; BBB; repair; EM

Introduction

Stroke is the fifth leading cause of death in the USA and someone dies of one approximately every 4 minutes [1]. Strokes occur due to interruption of blood flow to the brain and are typed as ischemic or hemorrhagic. Approximately 87% of strokes are ischemic [2]. The only FDA approved treatment for ischemic stroke is tissue plasminogen activator (tPA) for dissolving the blood clot and improving blood flow in the brain. Intravenous administration of tPA within 3 to 4.5 hours of stroke onset in selected patients with acute ischemic stroke [3] reduces mortality and increases rates of independent ambulation in living activities when thrombolytic treatment is given early after ischemic stroke [4]. However, since tPA is only available for acute ischemic stroke with a narrow therapeutic time window, treatment options for the majority of stroke patients are quite limited. Cell therapy, which targets the subacute, and even the chronic phase of the disease, shows promise as a novel treatment for stroke [5–10].

Various cell types such as bone marrow stromal cells [11–16], umbilical cord blood cells [17–19], or mesenchymal stem cells [20–22] administered systemically or locally have been proven functionally beneficial in rodent models of stroke, specifically middle cerebral artery occlusion (MCAO). Different mechanisms of cell actions have been posited to underlie the noted benefits including: increased neurotrophic growth factors in the ischemic tissue, reduced apoptosis in the penumbral lesion zone, reduced ischemic damage, and restored cerebral blood flow, altogether implicated in the functional recovery of post-MCAO animals [12–14, 16, 18–20]. Based on these encouraging pre-clinical results, limited clinical trials, mainly using autologous bone marrow-derived mesenchymal stem cells [22, 23] or mononuclear cells [24, 25], were initiated to treat patients with acute ischemic stroke. Positive functional outcomes in cell-treated patients suggested safety, but efficacy of the proposed treatments remains inconclusive [26]. Indeed, a recent meta-analysis [27] on seven clinical stroke studies, including those mentioned above, showed no significant differences between cell-treated and cell-free treated patients, suggesting that further research is needed to discover more effective stem cell-based therapies for ischemic stroke treatment.

To achieve this goal, we advanced the hypothesis that directed targeting of cell delivery into the injured vasculature might be a more feasible approach for stroke treatment. Numerous comprehensive studies have shown blood-brain barrier (BBB) damage in both ischemic stroke patients and MCAO-induced stroke animals [28–39]. Recently, we demonstrated BBB [40, 41] and blood-spinal cord barrier (BSCB) [42] alterations in brain and spinal cord areas

remote from the initial brain ischemic insult in a subacute and chronic rat model of MCAO. Since pervasive and persistent BBB impairment is an important factor in ischemic stroke pathogenesis, BBB repair might be considered a primary target for cell therapy development. An early study [12] demonstrated that intrastriatal transplantation of bone marrow stromal cells into MCAO rats dose-dependently restored local cerebral blood flow and decreased BBB permeability, mediating functional outcomes in stroke rats. Another study [11] using the same type of cells, administered intravenously into rats 24 hours after MCAO, showed significantly decreased BBB leakage and increased tight junction protein (occludin) expression in the ischemic border of cell-treated rats leading to vascular stabilization. However, endothelial progenitor cells (EPCs), due to their vascular phenotype, might be a more efficacious cell source for BBB restoration in stroke. It has been shown that intravenous administration of human-cord-blood-derived EPCs into rats 24 hours post-MCAO [43] or circulated human EPCs into nude mice 1 hour after MCAO [44] promoted angiogenesis and neurovascular repair foremost while also reducing ischemic infarct volume and improving neurobehavioral outcomes in treated animals. Also, transplantation of various cell doses from a human cerebral EC line (HEN6) into the striatum of rats at 3 hours post-tMCAO demonstrated robust vasculogenesis and neurogenesis in a dose-dependent manner potentially mediated by the VEGF signaling pathway [45]. Recognizing that the mechanism of action underlying the therapeutic benefits of cell therapy in stroke is still unclear, we embarked here in examining the effects of transplanted EPCs on mitochondria and pinocytosis, in view of recent reports implicating that their alterations contribute to BBB impairment in stroke [46, 47]. We hypothesize that grafted EPCs preserve mitochondrial morphology and promote pinocytic activity.

The aim of the present study was to evaluate exclusively by electron microscopy the effects of intravenously transplanted human bone marrow EPCs into MCAO rats in an effort to reveal the ultrastructure component, as well as functionality of stem cell-mediated BBB repair. A specific focus was determining capillary endothelium integrity in brain areas remote from the initial ischemic insult in cell-treated MCAO rats.

Materials and Methods

Ethics Statement

All described procedures were approved by the Institutional Animal Care and Use Committee at USF and were conducted in compliance with the NIH *Guide for the Care and Use of Laboratory Animals*.

Animals

All animals used in the study were obtained from The Jackson Laboratory, Bar Harbor, Maine. Sprague Dawley adult male rats weighing 252.6 ± 1.38 g were housed in a temperature-controlled room (23°C) and maintained on a 12:12 h dark: light cycle (lights on at 06:00 AM). Food and water were available *ad libitum*.

Middle Cerebral Artery Occlusion

Stroke surgery was performed on eight rats via transient middle cerebral artery occlusion (tMCAO) using the intraluminal filament technique previously described in detail [19, 40, 41, 48] and based on our prior standardization of this stroke model [49–51] showing at least an 80% reduction in regional cerebral blood flow in stroke animals during the occlusion period as determined by laser Doppler (Perimed). Briefly, the tip of the filament was customized using a dental cement (GC Corporation, Tokyo, Japan). Body temperature was maintained at 37 ± 0.3°C during the surgical procedures. A midline skin incision was made in the neck with subsequent exploration of the right common carotid artery (CCA), the external carotid artery, and internal carotid artery. A 4-0 monofilament nylon suture (27.0–28.0 mm) was advanced from the CCA bifurcation until it blocked the origin of the middle cerebral artery (MCA). Animals were allowed to recover from anesthesia during MCAO. At 60 minutes after MCAO, animals were re-anesthetized with 1–2% isoflurane in nitrous oxide/oxygen (69%/30%) using a face mask and reperfused by withdrawal of the nylon thread. A midline incision was made in the neck and the right CCA was isolated. The animals were then closed and allowed to recover from anesthesia.

Human Bone Marrow Endothelial Progenitor Cell Isolation

The isolation of human bone marrow endothelial progenitor cells (hBMEPCs) was performed accordingly to the protocol reported previously [52–54] with modifications. Briefly, for each independent experiment, human bone marrows (AllCells) were kept in Hank's Balanced Salt Solution (HBSS) (Sigma Aldrich). Under the hood, bone marrows were placed at 37°C for 15 min, and processed through a 40-μm nylon membrane (BD Biosciences) to obtain cell suspension. Mononuclear cells (MNCs) were obtained by density-gradient centrifugation with Ficoll® Paque Plus (Amersham Biosciences). Isolated MNCs were shortly washed with red blood cell lysis solution (Zonza) and then gently washed twice with complete growth media EGM-2MV (Lonza). MNCs were finally resuspended in EGM-2MV and 3×10^7 MNCs per well were seeded on collagen I-coated six-well plates (Becton Dickinson Labware) and incubated in a 5% CO2 incubator at 37 °C for 5–7 days in culture. Cells adherent to collagen I-coated dishes were largely mesenchymal-like cells (CD34 positive) and exhibited a spindle-shaped morphology in this culture condition. Under daily observation, the first media change was performed 3 days after plating. Early EPCs were used for each independent experiment between days 5 and 7 after seeding. The immunophenotyping of hBMEPCs was performed on day 5 after seeding. Direct fluorescent staining was used to detect lectin binding with FITC-labeled Ulex europaeus agglutinin (UEA)-1 (Sigma). In parallel, surface-antigen expressions of markers such as CD34, CD133 (Prominin-1), KDR (human vascular endothelial growth factor 2 receptor), and von Willebrand Factor (vWF) were performed using immunocytochemistry. All cells were counterstained with Vectashield® mounting media with DAPI (Vector Laboratories) and cells visualized with a fluorescent microscope. Adherent cells showing fluorescence for lectin and positivity for CD133, CD34, vWF, and KDR markers were identified as differentiating into early EPCs.[52–54] Quantification of specific immunofluorescent staining for each antibody was assessed by visualization under a Zeiss fluorescent microscope, using duplicates from three different batches of EPC isolation by two blinded observers. For estimation of immunofluorescent cells, randomly selected visual

fields were photographically captured (Axiophot2; Zeiss), and cells were quantified by counting per high-power field view also selected at random (duplicates from three different batches of EPC isolation, $n = 6$ in each group, 28,800 μm^2). Control studies involved exclusion of primary antibody substituted with 10% normal horse serum in PBS. No immunoreactivity was observed in these controls.

Labeling of hBMEPCs with β-galactosidase (β-gal) and Immunocytochemical Detection of β-gal-Positive Cells in vitro

To provide a sensitive molecular tag for identification of transplanted hBMEPCs, cells were infected with replication-incompetent retroviral vector encoding β-galactosidase (β-gal) and puromycin-resistant genes [55, 56], thereby producing β-gal-positive cells. For detection of pre-labeled hBMEPCs, immunocytochemistry was performed *in vitro*. Cultured cells were incubated with anti-β-gal primary antibody (1:200, Sigma) overnight at 4°C. Next day, cells were washed 3 times for 5 min with 0.1 M phosphate buffered saline (PBS, pH 7.2) and incubated with FITC-conjugated anti-mouse IgM antibody (1:300, Jackson Immunoresearch) for 1 hour at room temperature. Cells were visualized with a fluorescent microscope.

Cell Transplant Procedure

On the day of transplantation, β-gal-positive hBMEPCs were dissociated into single cells by brief trypsin treatment and suspended in PBS at 4×10^6 cells/ml and kept on ice until transplantation. The cell suspension was injected slowly for 5 minutes into the jugular vein of four randomly selected rats at 48 hours after tMCAO as we previously described [48, 57, 58].

Perfusion and Tissue Preparation

Five days after transplantation, cell-treated tMCAO and non-treated tMCAO rats were sacrificed under CO_2 inhalation and perfused transcardially with 0.1 M phosphate buffer (PB, pH 7.2) followed by 4% paraformaldehyde (PFA) in PB solution under pressure controlled fluid delivery at 85 mm Hg. Three control rats were also sacrificed at the same time. Rat brains were immediately removed, labeled on left hemisphere, and fixed in 4% PFA in 0.1 M PB for 16–24 hours at 4°C. The next day, brains were cut into 1 mm slices, mapped against a diagram of the whole slice at Bregma level of 0.20–0.48 mm according to a rat brain atlas [59].

For electron microscopy detection of transplanted pre-labeled hBMEPCs with β-gal, horseradish peroxidase followed by 3,3'-diaminobenzidine (HRP-DAB) staining was performed as described [60] by omitting the secondary antibody. Briefly, the slices were washed 3 times for 5 min with 0.1 M PBS and incubated with a streptavidin-HRP solution (Vectastain® Elite ABC kit, Vector Laboratories) for 1 hour at room temperature. After washing slices 3 times for 5 min with PBS, DAB solution (Thermo Scientific) was applied to the brain slices for 3–5 min. Following HRP-DAB staining, slices were rinsed in PBS (3 × 10 min) to remove non-specific staining.

Electron Microscopy

After HRP-DAB staining, brain slices from cell-treated, non-treated, and control rats were post-fixed in 2.5% glutaraldehyde in 0.1M PB (Electron Microscopy Sciences, Inc., Hatfield, PA) at 4°C overnight. Following thorough buffer rinsing, slices were then osmicated in 1% osmium tetroxide in the above buffer. Osmium tetroxide fixation renders the HRP-DAB stain reaction product visible in the electron microscope as an insoluble precipitate, labeling the transplanted stem cells and making them visible for the transmission electron microscopy [61, 62]. The tissue slices were dissected into ipsilateral and contralateral sides and the motor cortex (M1/M2) and striatum (CPu) regions were removed and coded from the slices of both brain hemispheres from each group for separate processing as we previously described [41]. Coordinates for ipsi- M1/M2 motor cortex area were about 4 mm ventral and 1.5 mm lateral from the striatum on the coronal section according to a rat brain atlas [59]. The same coordinates were applied for removal of striatum and motor cortex tissues from the contralateral hemisphere. After osmication, samples were thoroughly rinsed in distilled water. Samples were then dehydrated in a graded series of acetone solutions, then infiltrated and embedded in LX-112 epoxy embedding resin. Following polymerization, tissue blocks were sectioned, and sections were stained with 8% aqueous uranyl acetate and Reynold's lead citrate stains.

BBB Integrity Analysis

For analysis of BBB ultrastructure, microvessels in the ipsilateral and contralateral the striatum and motor cortex regions of cell-treated tMCAO, non-treated tMCAO rats and their controls were examined by an investigator blinded to the animal groups, using mapped/coded sections, and photographed on an FEI Morgagni transmission electron microscope (TEM) (FEI, Corp., Hillsboro, OR) at 60kV using an Olympus MegaView III camera (ResAlta, INC., Golden, CO). More than fifty EM images were taken of striatum and of motor cortex in ipsilateral and contralateral brain hemispheres from each animal.

Vesicle sizes within ECs were measured using analySIS software by Olympus Soft Imaging System (GmbH, Munster, Germany). The measurements of vesicle size are presented in nm. Additionally, the number of vesicles was counted within ECs from randomly selected (by a blinded investigator) EM images of microvessels in the ipsilateral and contralateral striatum and motor cortex regions of cell-treated tMCAO rats (n=8/structure/side).

Mitochondrial morphology within ECs and perivascular astrocytes was examined in randomly selected (by a blinded investigator) EM images of microvessels in the ipsilateral and contralateral striatum and motor cortex regions of cell-treated tMCAO, non-treated tMCAO and control rats (n=6–7/group/structure/side). The counts of mitochondria with normal and abnormal (swollen, disrupted cristae, or degenerated) morphologies are presented as percentages of total mitochondria.

Statistical Analysis

Data are presented as means ± S.E.M. One-way ANOVA with Tukey's Multiple Comparison test using GraphPad Prism software version 5 (GraphPad Software) was performed for statistical analysis. Significance was defined as $p < 0.05$.

Results

Immunocytochemical Characteristics of Isolated hBMEPCs and Labeled Cells with β-galactosidase (β-gal) in vitro

Isolated MNCs from human bone marrow began to attach to collagen I-coated plates at Day 1 *in vitro* (Figure 1A). Adherent cells were characterized by conglobate cell bodies with clear cytoplasm under specific culture condition. At Day 3, cultured cells displayed mesenchymal-like cell morphology and exhibited spindle-shapes with some cell-to-cell networks and formed small colonies. At Days 5–7, more cells continued to form larger colonies and cell networks with about 80% reaching confluence with the characteristic cobblestone-like monolayer. Using fluorescent immunostaining at Day 5 of culture, early human bone marrow-derived EPCs showed positive for CD133, VEGF-2 (KDR), and vWF, revealing 86%, 76%, and 82% positivity for each marker, respectively (Figure 1B). Labeling of hBMEPCs with β-gal produced >90% β-gal-positive cells (Figure 1C).

Ultrastructure of the Cerebral Microvasculature in Ischemic tMCAO Rats after hBMEPCs Transplantation

The effect of intravenous transplantation of β-gal pre-labeled hBMEPCs into rats at 48 hours after tMCAO on BBB repair was analyzed in brains of rats sacrificed 5 days post-transplant (7 days post-tMCAO) using electron microscopy. Ultrastructural analysis of microvessels in the striatum and motor cortex of the brain was performed on hemispheres ipsilateral and contralateral to tMCAO damage in cell-treated animals in comparison to non-treated tMCAO and control rats (n=4). One animal did not survive 24 hours after tMCAO and another animal died shortly after cell transplantation. These rats were excluded from our study.

Striatum

The striatum of control rats was characterized by normal ultrastructural appearance of capillaries, neurons, neuropil, myelinated axons, and surrounding astrocytes (Figure 2A, B, C). Capillaries consisted of a single layer of endothelial cells (ECs) with clearly apparent tight junction. The ECs were surrounded by a layer of basement membrane (BM) and pericyte processes. Organelles in all cells were well preserved and mitochondria demonstrated normal cristae.

In the hemisphere ipsilateral to tMCAO of stroke animals that did not receive the transplants, 7 days after insult, ultrastructural abnormalities were observed in capillary endothelia in striatum (Figure 2D, E). Necrotic EC with condensed cytoplasm was adjacent to a swollen EC (Figure 2D). ECs showed formation of numerous large vacuoles and swollen mitochondria with disrupted cristae in their cytoplasm (Figure 2E). Cell processes of degenerated pericytes surrounding the capillary were observed. Large perivascular protein-filled areas (edema) created by degenerated astrocyte cell processes were common. In contralateral striatum, less severe, but still significant, vascular damage was observed. Capillary contains a necrotic EC (Figure 2F) or a swollen EC (Figure 2G). Some areas of edema surrounding the capillaries were detected. A capillary (Figure 2G) displayed a swollen EC layer containing enlarged vacuolated mitochondria and autophagosomes.

Five days after hBMEPC transplantation, numerous capillaries in striatum ipsilateral to tMCAO insult demonstrated normal ultrastructural morphology consisting of microvessels with EC layer in dark color revealing engraftment of β-gal pre-labeled hBMEPCs using the HRP-DAB stain (Figure 2H, I). The ECs displayed numerous pinocytic vesicles near abluminal and luminal cell membranes indicating pinocytosis. There was no evidence of perivascular edema. Healthy pericytes and typical appearance of neurons and astrocytes were noted. Mitochondria in ECs and astrocyte end-feet also showed a normal pattern of cristae. In contralateral striatum (Figure 2J, K), a number of vesicles in ECs were visible, although fewer were noted here compared to ipsilateral-hemisphere capillaries. A lack of perivascular edema was also determined in these remote capillaries. There was normal ultrastructural appearance of capillaries, pericytes, and surrounding astrocytes. Significantly ($p < 0.001$) more pinocytic vesicles were detected in capillary ECs from ipsilateral than contralateral hemisphere in striatum (ipsilateral – 103.38 ± 6.40, contralateral – 51.29 ± 4.57) from cell-treated tMCAO rats (Figure 2L). There were no pinocytic vesicles identified within brain capillaries in non-treated tMCAO or control rats.

Motor Cortex

Similar to striatum, capillaries in control motor cortex showed typical ultrastructure, consisting of vessels with a single layer of endothelium, surrounded by BM and astrocyte cell processes (Figure 3A, B, C). A tight junction was clearly visible between ECs (Figure 3B). Neuron with centered nucleus was apparent with normal cellular morphology (Figure 3C). In non-treated stroke animals, the hemisphere ipsilateral to tMCAO at 7 days after insult showed numerous capillaries containing necrotic ECs with condensed cytoplasm adjacent to a swollen EC and/or a healthy EC in the lumen (Figure 3D). Extensive perivascular edema separating astrocyte end-feet from capillary was evident (Figure 3D, E). A lysosome with black lipid membranes indicating digestion of lipids in EC was determined (Figure 3E). Also, large swollen mitochondria in EC cytoplasm and in degenerated pericyte were visible in this capillary. In contralateral motor cortex, capillaries showed endothelial and pericyte cell damage similar to ultrastructural capillary abnormalities in ipsilateral cortex (Figure 3F, G). A number of capillaries contained necrotic ECs (Figure 3F, G). Autophagosome formation was also observed in the cytoplasm of swollen EC (Figure 3F). Perivascular edema surrounding the capillaries and degenerated pericytes were seen in represented images.

Five days after hBMEPC transplantation, numerous capillaries in the motor cortex ipsilateral to tMCAO insult exhibited normal ultrastructural morphology of ECs and were characterized by healthy pericytes, myelinated axons, and astrocyte processes surrounding vessels (Figure 3H, I). Tight junctions between ECs were clearly detected (Figure 3I). Similar to striatum capillaries, ECs in motor cortex displayed numerous pinocytic vesicles, mainly at abluminal cell membranes (Figure 3H, I). Importantly, a healthy pericyte also showed cytoplasmic vesicles (Figure 3H). There was no evidence of perivascular edema. In contralateral motor cortex, vesicles in ECs were also visible but to a lesser degree compared to capillaries in the ipsilateral hemisphere (Figure 3J, K). Also, perivascular edematous areas were not identified. There was normal ultrastructural appearance of capillaries, surrounding astrocytes end-feet, pericytes, and myelinated axons. Similarly to striatum, significantly ($p <$

0.001) higher numbers of pinocytic vesicles in motor cortex capillary ECs were determined in ipsilateral (91.43 ± 5.27) vs. contralateral (53.00 ± 1.58) hemisphere with no pinocytosis detected in non-transplant tMCAO or control rats (Figure 3L). Of note, sizes of pinocytic vesicles from randomly selected capillaries in the striatum and motor cortex in both ipsilateral and contralateral hemispheres of hBMEPC-treated tMCAO rats were remarkably uniform at 69.44 ± 2.71 nm from a total of 36 counted vesicles.

Morphological Characteristics of Mitochondria in Endothelial Cells and Perivascular Astrocytes

The morphology of mitochondria was analyzed in ECs and perivascular astrocytes in hBMEPC-treated tMCAO, non-treated tMCAO, and control rats. Mitochondria with normal and abnormal (swollen, disrupted cristae, or degenerated) morphologies were examined in ipsilateral and contralateral hemispheres in both striatum and motor cortex and presented as percentages of total mitochondria. Since mitochondria counts in control rats were similar in ipsilateral and contralateral hemispheres in both striatum and motor cortex, data were presented as averages in analyzed brain structures for these animals. Results showed significant ($p < 0.001$) reduction of mitochondrial percentages with normal morphology within ECs in ipsilateral and contralateral hemispheres in both striatum (control – 96.97 ± 0.37%, tMCAO ipsi- -- 87.52 ± 1.36%, tMCAO contra- -- 90.23 ± 1.02%) and motor cortex (control – 96.50 ± 0.61%, tMCAO ipsi- -- 87.07 ± 0.81%, tMCAO contra- -- 89.83 ± 1.28%) of non-treated tMCAO rats at 7 days after insult (Figure 4A). Similarly, a significant ($p < 0.001$) decrease of normal mitochondria was noted in perivascular astrocytes of tMCAO rats in striatal and cortical areas of ipsilateral and contralateral hemispheres (striatum: control – 94.02 ± 0.66%, tMCAO ipsi- -- 81.18 ± 1.53%, tMCAO contra- -- 88.74 ± 1.58%; cortex: control – 97.67 ± 0.74%, tMCAO ipsi- -- 83.01 ± 2.00%, tMCAO contra- -- 85.48 ± 1.70%) (Figure 4B). Interestingly, the percentage of mitochondria with normal morphology was higher in contralateral vs. ipsilateral hemisphere of striatum ($p < 0.001$) in stroke animals, but it was still significantly ($p < 0.05$) lower than in control rats. In hBMEPC-treated tMCAO rats, significant increases of normal mitochondrial percentages within ECs were detected in ipsilateral hemisphere ($p < 0.001$) of the striatum (93.39 ± 0.97%) and cortex (94.81 ± 0.61%) as well as in the contralateral (striatum: 94.66 ± 0.50%, cortex: 94.64 ± 0.63%) hemisphere ($p < 0.01$) vs. non-treated tMCAO rats (Figure 4A). A significantly ($p < 0.001$) greater percentage of normal mitochondria was also demonstrated in perivascular astrocytes in ipsilateral hemisphere of both striatum and motor cortex of cell-treated vs. non-treated tMCAO rats (Figure 4B). In the contralateral hemisphere, significant differences between hBMEPC-treated and non-treated tMCAO rats were detected only in cortical areas ($p < 0.05$).

Since significant decreases of mitochondria with normal morphology within ECs and perivascular astrocytes were detected in ipsilateral and contralateral hemispheres in both striatum and motor cortex of tMCAO rats, analysis of abnormal mitochondrial morphology was performed. In ECs, significantly ($p < 0.001$) higher percentages of swollen mitochondria, mitochondria with disrupted cristae and degenerated mitochondria was shown in ipsilateral hemisphere in striatum (swollen: 6.62 ± 1.02%, disrupted cristae: 3.42 ± 0.67%, degenerated: 2.44 ± 0.43%) and motor cortex (swollen: 7.26 ± 0.72%, disrupted

cristae: 2.48 ± 0.33%, degenerated: 3.19 ± 0.45%) of non-treated tMCAO rats vs. controls (Figure 4C). In contralateral hemisphere of analyzed brain structures of stroke animals, an increase of mitochondria with abnormal morphology was also demonstrated with different degree of significance. After hBMEPC treatment of tMCAO rats, percentages of abnormal mitochondria in ECs were reduced for all distinguished morphologies, however, significance was determined only in ipsilateral cortex for swollen mitochondria ($p < 0.001$). Degenerated mitochondria were almost undetectable in ECs of treated animals and showed significant differences compared to tMCAO rats in ipsilateral ($p < 0.001$) and contralateral ($p < 0.01$) striatum as well as in ipsilateral ($p < 0.001$) and contralateral ($p < 0.05$) cortex (Figure 4C). Compelling profile of abnormal mitochondrial morphology in perivascular astrocytes demonstrated higher percentages of mitochondria with disrupted cristae in ipsilateral and contralateral hemispheres in both striatum (ipsi-: 10.46 ± 1.12%, contra-: 6.49 ± 1.27%) and motor cortex (ipsi-: 9.33 ± 1.12%, contra-: 9.51 ± 1.65%) of tMCAO rats vs. controls (striatum: 2.81 ± 0.45%, cortex: 2.65 ± 0.37%) (Figure 4D). Significant increases of swollen mitochondria were only detected in ipsilateral striatum ($p < 0.001$) and cortex ($p < 0.05$). Regarding degenerated mitochondria, similar findings were shown in ipsilateral striatum ($p < 0.01$) and cortex ($p < 0.05$). Of note, degenerated mitochondria in contralateral striatum were significantly less ($p < 0.05$) vs. ipsilateral hemisphere in tMCAO rats. Percentages of perivascular astrocyte mitochondria with abnormal morphology were reduced in ipsilateral and contralateral hemispheres of striatum and motor cortex of hBMEPC-treated tMCAO rats, however, significant differences were detected only in ipsilateral striatum ($p < 0.01$) and ipsi-/contralateral cortex ($p < 0.05$) for mitochondria with disrupted cristae (Figure 4D). Degenerated mitochondria were significantly decreased in ipsilateral striatum ($p < 0.01$) and cortex ($p < 0.001$) in cell-treated vs. stroke animals.

Discussion

In the present study, we investigated the effects of intravenously transplanted β-gal pre-labeled hBMEPCs into rats at 48 hours after tMCAO on BBB repair using electron microscopy. Transmission electron microscopy is the exclusive method for visualizing cell/tissue eminence including intracellular organelles and cytoskeleton in the CNS at high spatial resolution. Ultrastructural analysis of microvessels was performed at 5 days post-transplant in the striatum and motor cortex of the brain hemispheres ipsilateral and contralateral to tMCAO damage. Our results demonstrated vascular repair in brain structures of both hemispheres via transplanted cell engraftment into the vascular wall that appeared to re-establish BBB integrity post-stroke. The major findings supporting BBB repair in cell-treated tMCAO rats included: (1) extensive vascular engraftment of β-gal pre-labeled hBMEPCs, (2) normal ultrastructural morphology of ECs, healthy pericytes, myelinated axons, and astrocyte processes surrounding vessels, (3) significant increase of mitochondria with normal morphology and decrease of abnormal mitochondria within engrafted EC and perivascular astrocytes, (4) lack of perivascular edema, (5) numerous pinocytic vesicles at abluminal and luminal membranes of engrafted hBMEPCs with significantly more vesicles in ipsilateral than contralateral hemisphere. These data suggest successful hBMEPC incorporation and engraftment into the vascular wall not only in the ipsilateral but also in contralateral remote brain areas. Importantly, the formation of numerous vesicles indicating

pinocytotic activity in hBMEPCs suggests high functionality of engrafted cells. Interestingly, we report here that intravenously transplanted hBMEPCs in tMCAO rats successfully engrafted into the cerebrovasculature and exerted pinocytotic activity which might have mediated the restoration of the BBB after stroke. This BBB repair was observed in the early phase of stroke, thereby warranting additional studies designed to examine robust and stable long-term post-transplant effects on restoration of BBB.

The BBB damage in the ipsilateral and contralateral striatum and motor cortex observed at the ultrastructural level at 7 days post-tMCAO (time of evaluation of post-transplant effect) was consistent with our previous results [40] demonstrating subacute diaschisis in tMCAO rats. Microvascular injury characterized by capillary EC damage, pericyte and astrocyte degeneration, and perivascular edema in observed brain areas are significant pathologies identifying compromised BBB integrity in non-treated tMCAO animals from the present study. In hBMEPC-treated tMCAO rats, these stroke-induced BBB pathologies were undetected. Engraftment of transplanted β-gal pre-labeled hBMEPCs was confirmed in numerous cerebral capillaries in both brain hemispheres by EM after HRP-DAB staining followed by osmication. Osmium tetroxide fixation renders the HRP-DAB stain reaction product visible to the electron microscope as an insoluble precipitate, allowing EM identification of β-gal pre-labeled cells [61, 62]. Since DAB reacts with osmium tetroxide stain during fixation for EM, transplanted cells should show a dark stain, differentiating them from the surrounding cell/tissue. Thus, a single HRP-DAB staining of β-gal pre-labeled hBMEPCs is sufficient for EM analysis *in vivo*. Moreover, immunohistochemical detection of pre-labeled hBMEPCs was confirmed *in vitro* prior to cell transplantation. However, double immunostaining for CD133 and VEGFR2 to identify EPC positive cells will be included in our future studies. Interestingly, pericytes, by nature, take in more osmium tetroxide than surrounding cell/tissue, thereby eliciting a dark color due to their high levels of cytoplasmic proteins. However, the cytoplasm in pericytes was still lighter than the β-gal pre-labeled hBMEPCs in our EM images.

The beneficial effect of intravenously transplanted hBMEPCs in tMCAO rats was also evidenced by quantitative mitochondrial morphology analysis within ECs and perivascular astrocytes at ultrastructural level. Mitochondria are essential cellular organelles with multiple roles in maintaining cell homeostasis. The mitochondrion is the primary cellular energy supplier producing adenosine triphosphate [63] and is involved in cell cycle and growth [64]. This organelle also has a central role in cellular metabolism by regulation of calcium [65], mitochondrial membrane potential [63], reactive oxygen species [66], and apoptosis [67]. Mitochondrial alterations could lead to cellular energy deficit or oxidative stress, resulting in cell death. We [68–70] and others [71–74] have demonstrated mitochondrial dysfunction after experimental stroke. Mitochondrial dysfunction following stroke has been associated with reduced number and size of mitochondria in astrocytes [75], neuronal mitochondrial swelling and fragmentation [72, 76], excitotoxic calcium entry overload [77], and deficient astrocytic support to neuronal functions [78]. Although mitochondrial morphological status in neurons was not evaluated in the current study, our results generally supported previous findings on post-stroke mitochondrial alterations in astrocytes [75, 78]. We further demonstrated that following stroke significantly fewer mitochondria with normal morphology in perivascular astrocytes not only in ipsilateral, but

also in contralateral striatum and motor cortex. Mitochondria with disrupted cristae were the main contributors to pathological condition of astrocytes, while swollen mitochondria were also highly determined. Potentially, these dysfunctional mitochondria led to astrocyte end-feet degeneration, which exacerbated post-ischemic BBB damage. Convincing evidence of compromised BBB integrity in non-treated tMCAO animals was provided in our study by demonstrating significant reduction of mitochondria with normal morphology in ECs. In contrast to perivascular astrocyte mitochondria, the significantly higher percentage of swollen mitochondria in ECs points to an abnormal mitochondrial profile in post-stroke animals. In our previous study [40] showing subacute diaschisis in tMCAO rats, microvascular injury was mainly characterized by capillary EC damage in both the ipsilateral and contralateral striatum and motor cortex. Adding knowledge regarding the role of mitochondria in post-stroke EC degeneration by categorizing their abnormal morphologies might lead to the use of mitochondrial condition as a potential biomarker of BBB alterations after stroke as well as for determining treatment effect(s). On the other hand, targeting mitochondria *per se* might be a potent therapeutic approach for stroke [68–70, 72–74, 79]. In fact, we showed that intravenous transplantation of hBMEPCs into tMCAO rats significantly decreased abnormal mitochondria, resulting in increased numbers of mitochondria with normal morphology within ECs and perivascular astrocytes. However, functional assays such as mitochondrial electron transport chain complexes or mitochondrial membrane potential, might allow correlation of specific mitochondrial aberrations with altered mitochondrial functionality. However, it is still unclear if mitochondrial dysfunction plays a primary or secondary role in the cascade of events leading to BBB impairment in stroke. These and other studies are planned for the near future.

The most novel finding in our study is the appearance of numerous pinocytic vesicles solely in engrafted hBMEPCs of cell-treated post-tMCAO animals. Normally, adult brain capillary ECs lack pinocytic vesicles [80–82], which is believed to be the cause of low BBB permeability by inhibiting transcellular passage of molecules across the barrier [83, 84]. EC pinocytic vesicles functionally differ from other intracellular vesicle types such as endocytic vesicles (endosomes) in the process of endocytosis, which mainly involves transcellular passage of macromolecules between the blood and the brain. Although the BBB prevents many macromolecules from entering the brain, a variety of macromolecules such as proteins and peptides might cross the cerebral endothelium via receptor-mediated or adsorptive-mediated transcytosis [85, 86] by uptake of material into a cell by an invagination of the plasma membrane and its internalization in a membrane-bounded vesicle. Both types of transcytosis use a vesicular-based system e.g. endocytosis [87, 88]. Pinocytosis, “cellular drinking” or “fluid-phase endocytosis”, involves the ingestion of fluid and/or soluble materials from the environment and these solutes are then incorporated into small pinocytic vesicles (about 100 nm in diameter) for digestion or passage [89].

The pinocytic vesicles, found only in engrafted hBMEPCs within cerebral capillaries of cell-treated post-tMCAO animals, represent an innovative line of investigation in the field of cell therapy. Sizes of the vesicles observed in our study, at approximately 70 nm in diameter, roughly agree with previous observation [72]. We posit that administered stem cells, such as EPCs derived from human bone marrow, undergo *in vivo* proliferation, differentiation, maturation, migration, and adherence to host stroke damaged capillaries. Upon completion

of these processes, in our case 5 days post-transplant, when cells engrafted (homed) into the vascular wall, pinocytic activity in these cells is advent and might indicate high functionality of newly introduced cells in replacement of damaged ECs. Also, the absence of perivascular edema at the site of vesicles' appearance at abluminal membranes of engrafted hBMEPCs is evidence that transplanted cells used pinocytosis for rapid draining fluid from the damaged brain in capillary areas where they have incorporated. Since more BBB damage occurred in the ipsilateral than in contralateral hemisphere at 7 days post-tMCAO, as observed in the present and previous study [40], the significantly higher number of pinocytic vesicles detected in engrafted hBMEPCs in ipsilateral vs. contralateral hemisphere in both striatum and motor cortex supports the importance of pinocytic activity in post-stroke microvascular recovery. Of note, pinocytosis was noted only in newly grafted cells within capillaries.

Although we advance the concept that intravenously transplanted hBMEPCs replaced post-stroke damaged ECs, it is possible that administered cells were involved in capillary sprouting or might have extravasated to the brain parenchyma via paracellular migration across cell-cell junctions similarly to leukocyte diapedesis in various pathological conditions [82, 84, 90] given the new vessel formation. Transplanted hBMEPCs might promote neovascularization and/or stimulate angiogenesis in ischemia-damaged cerebral areas [43, 44], enhancing BBB integrity. Moreover, since BSCB damage has also been shown [42] in a rat model of ischemic stroke, determining the effects of transplanted cells on repair of this barrier in the spinal cord is important for confirming vascular restoration in areas remote from initial tMCAO insult. Also, defining BBB permeability after cell transplantation is essential to confirm the benefit of our proposed stroke treatment, which is being addressed in on-going studies. The involvement of EPCs in re-endothelialization during the neovascularization or formation of collateral vessels after ischemia has been discussed in comprehensive reviews [91–95] emphasizing safety and efficacy approaches of EPCs for future clinical applications in stroke patients [10, 96, 97].

Additionally, transplanted hBMEPCs might not only exogenously but also endogenously enhance post-stroke vasculogenesis via secretion of angiogenic or growth factors. Ishikawa et al. [45] showed that local transplantation of human EC cell line improved endogenous vasculogenesis and neurogenesis by the VEGF signaling pathway. Significantly increased angiogenesis and neurogenesis were recently shown in MCAO mice treated with murine BMEPCs mediated via the endothelial nitric oxide synthase (eNOS)/brain-derived neurotrophic factor (BDNF) signaling pathway [98]. Our future studies will address this possibility.

Altogether, the results revealed that intravenously transplanted β-gal pre-labeled hBMEPCs into rats 48 hours after tMCAO engrafted within the capillary wall at 5 days after administration, indicating the close involvement of the transplanted cells in vasculature repair of the BBB in subacute stroke. Ultrastructural analysis of microvessels, in the bilateral striatum and motor cortex of animals with unilateral ischemic stroke, identified rampant pinocytotic vesicles, which are very uncommon in adult brain capillary ECs, but recognized in ECs of cell-treated stroke animals. In tandem with the preservation of normal mitochondrial morphology, the observation of BBB repair by newly engrafted hBMEPCs opens a new avenue of research towards a better understanding of disease pathology and

treatment, in particular for the development of cell-based therapeutics directed at enhancing mitochondrial function and pinocytotic activity in stroke.

Supplementary Material

Refer to Web version on PubMed Central for supplementary material.

Acknowledgments

Funding

The author(s) disclosed receipt of the following financial support for the research, authorship, and/or publication of this article:

This study was supported by the NIH (1RO1NS071956-01A1) and the James and Esther King Biomedical Research Program (1KG01-33966).

References

1. Mozaffarian D, Benjamin EJ, Go AS, et al. Heart disease and stroke statistics--2015 update: a report from the American Heart Association. Circulation. 2015; 131:e29–e322. [PubMed: 25520374]
2. Go AS, Mozaffarian D, Roger VL, et al. Heart disease and stroke statistics--2013 update: a report from the American Heart Association. Circulation. 2013; 127:e6–e245. [PubMed: 23239837]
3. del Zoppo GJ, Saver JL, Jauch EC, et al. Expansion of the Time Window for Treatment of Acute Ischemic Stroke With Intravenous Tissue Plasminogen Activator. Stroke. 2009; 40:2945–2948. [PubMed: 19478221]
4. Saver JL, Fonarow GC, Smith EE, et al. Time to treatment with intravenous tissue plasminogen activator and outcome from acute ischemic stroke. JAMA. 2013; 309:2480–2488. [PubMed: 23780461]
5. Bliss T, Guzman R, Daadi M, et al. Cell transplantation therapy for stroke. Stroke. 2007; 38(2 Suppl):817–826. [PubMed: 17261746]
6. Pellegrini L, Bennis Y, Guillet B, et al. [Cell therapy for stroke: from myth to reality]. Rev Neurol (Paris). 2013; 169:291–306. [PubMed: 23246427]
7. Gopurappilly R, Pal R, Mamidi MK, et al. Stem cells in stroke repair: current success and future prospects. CNS Neurol Disord Drug Targets. 2011; 10:741–756. [PubMed: 21838668]
8. Popa-Wagner A, Filfan M, Uzoni A, et al. Poststroke Cell Therapy of the Aged Brain. Neural Plast. 2015; 2015:839638. [PubMed: 26347826]
9. Savitz SI. Developing Cellular Therapies for Stroke. Stroke. 2015; 46:2026–2031. [PubMed: 26045599]
10. Borlongan CV. Cell therapy for stroke: remaining issues to address before embarking on clinical trials. Stroke. 2009; 40(3 Suppl):S146–S148. [PubMed: 19064801]
11. Zacharek A, Chen J, Cui X, et al. Angiopoietin1//Tie2 and VEGF//Flk1 induced by MSC treatment amplifies angiogenesis and vascular stabilization after stroke. J Cereb Blood Flow Metab. 2007; 27:1684–1691. [PubMed: 17356562]
12. Borlongan CV, Lind JG, Dillon-Carter O, et al. Bone marrow grafts restore cerebral blood flow and blood brain barrier in stroke rats. Brain Res. 2004; 1010:108–116. [PubMed: 15126123]
13. Li Y, Chen J, Chen XG, et al. Human marrow stromal cell therapy for stroke in rat: neurotrophins and functional recovery. Neurology. 2002; 59:514–523. [PubMed: 12196642]
14. Li Y, Chen J, Wang L, et al. Treatment of stroke in rat with intracarotid administration of marrow stromal cells. Neurology. 2001; 56:1666–1672. [PubMed: 11425931]
15. Li Y, Chopp M, Chen J, et al. Intrastriatal transplantation of bone marrow nonhematopoietic cells improves functional recovery after stroke in adult mice. J Cereb. Blood Flow Metab. 2000; 20:1311–1319. [PubMed: 10994853]

16. Yang B, Migliati E, Parsha K, et al. Intra-arterial delivery is not superior to intravenous delivery of autologous bone marrow mononuclear cells in acute ischemic stroke. Stroke. 2013; 44:3463–3472. [PubMed: 24114454]
17. Vendrame M, Cassady J, Newcomb J, et al. Infusion of human umbilical cord blood cells in a rat model of stroke dose-dependently rescues behavioral deficits and reduces infarct volume. Stroke. 2004; 35:2390–2395. [PubMed: 15322304]
18. Chen J, Sanberg PR, Li Y, et al. Intravenous administration of human umbilical cord blood reduces behavioral deficits after stroke in rats. Stroke. 2001; 32:2682–2688. [PubMed: 11692034]
19. Borlongan CV, Hadman M, Sanberg CD, et al. Central nervous system entry of peripherally injected umbilical cord blood cells is not required for neuroprotection in stroke. Stroke. 2004; 35:2385–2389. [PubMed: 15345799]
20. Lim JY, Jeong CH, Jun JA, et al. Therapeutic effects of human umbilical cord blood-derived mesenchymal stem cells after intrathecal administration by lumbar puncture in a rat model of cerebral ischemia. Stem Cell Res Ther. 2011; 2:38. [PubMed: 21939558]
21. Walczak P, Zhang J, Gilad AA, et al. Dual-modality monitoring of targeted intraarterial delivery of mesenchymal stem cells after transient ischemia. Stroke. 2008; 39:1569–1574. [PubMed: 18323495]
22. Bang OY, Lee JS, Lee PH, et al. Autologous mesenchymal stem cell transplantation in stroke patients. Ann Neurol. 2005; 57:874–882. [PubMed: 15929052]
23. Lee JS, Hong JM, Moon GJ, et al. A long-term follow-up study of intravenous autologous mesenchymal stem cell transplantation in patients with ischemic stroke. Stem Cells. 2010; 28:1099–1106. [PubMed: 20506226]
24. Moniche F, Gonzalez A, Gonzalez-Marcos J-R, et al. Intra-arterial bone marrow mononuclear cells in ischemic stroke: a pilot clinical trial. Stroke. 2012; 43:2242–2244. [PubMed: 22764211]
25. Prasad K, Sharma A, Garg A, et al. Intravenous autologous bone marrow mononuclear stem cell therapy for ischemic stroke: a multicentric, randomized trial. Stroke. 2014; 45:3618–3624. [PubMed: 25378424]
26. Borlongan CV. Age of PISCES: Stem cell clinical trials in stroke. Lancet. 2016; 388:736–738. [PubMed: 27497863]
27. Wang Q, Duan F, Wang M-X, et al. Effect of stem cell-based therapy for ischemic stroke treatment: A meta-analysis. Clin Neurol Neurosurg. 2016; 146:1–11. [PubMed: 27131124]
28. del Zoppo GJ, Hallenbeck JM. Advances in the vascular pathophysiology of ischemic stroke. Thromb Res. 2000; 98:73–81.
29. del Zoppo GJ, Mabuchi T. Cerebral microvessel responses to focal ischemia. J Cereb Blood Flow Metab. 2003; 23:879–894. [PubMed: 12902832]
30. Persidsky Y, Ramirez SH, Haorah J, et al. Blood-brain barrier: structural components and function under physiologic and pathologic conditions. J Neuroimmune Pharmacol. 2006; 1:223–236. [PubMed: 18040800]
31. Sandoval KE, Witt KA. Blood-brain barrier tight junction permeability and ischemic stroke. Neurobiol Dis. 2008; 32:200–219. [PubMed: 18790057]
32. Jin R, Yang G, Li G. Molecular insights and therapeutic targets for blood-brain barrier disruption in ischemic stroke: critical role of matrix metalloproteinases and tissue-type plasminogen activator. Neurobiol Dis. 2010; 38:376–385. [PubMed: 20302940]
33. Dankbaar JW, Hom J, Schneider T, et al. Dynamic perfusion-CT assessment of early changes in blood brain barrier permeability of acute ischaemic stroke patients. J Neuroradiol. 2011; 38:161–166. [PubMed: 20950860]
34. Preston E, Sutherland G, Finsten A. Three openings of the blood-brain barrier produced by forebrain ischemia in the rat. Neurosci Lett. 1993; 149:75–78. [PubMed: 8469386]
35. Yang GY, Betz AL. Reperfusion-induced injury to the blood-brain barrier after middle cerebral artery occlusion in rats. Stroke. 1994; 25:1658–1664. 1665. [PubMed: 8042219]
36. Belayev L, Busto R, Zhao W, et al. Quantitative evaluation of blood-brain barrier permeability following middle cerebral artery occlusion in rats. Brain Res. 1996; 739:88–96. [PubMed: 8955928]

37. Kuroiwa T, Ting P, Martinez H, et al. The biphasic opening of the blood-brain barrier to proteins following temporary middle cerebral artery occlusion. Acta Neuropathol. 1985; 68:122–129. [PubMed: 3907257]
38. Strbian D, Durukan A, Pitkonen M, et al. The blood-brain barrier is continuously open for several weeks following transient focal cerebral ischemia. J Neurosci. 2008; 153:175–181.
39. Abo-Ramadan U, Durukan A, Pitkonen M, et al. Post-ischemic leakiness of the blood-brain barrier: a quantitative and systematic assessment by Patlak plots. Exp Neurol. 2009; 219:328–333. [PubMed: 19520075]
40. Garbuzova-Davis S, Rodrigues MCO, Hernandez-Ontiveros DG, et al. Blood-brain barrier alterations provide evidence of subacute diaschisis in an ischemic stroke rat model. Plos ONE. 2013; 8:e63553. [PubMed: 23675488]
41. Garbuzova-Davis S, Haller E, Williams SN, et al. Compromised blood-brain barrier competence in remote brain areas in ischemic stroke rats at chronic stage. J Comp Neurol. 2014; 522:3120–3137. [PubMed: 24610730]
42. Garbuzova-Davis S, Haller E, Tajiri N, et al. Blood-Spinal Cord Barrier Alterations in Subacute and Chronic Stages of a Rat Model of Focal Cerebral Ischemia. J Neuropathol Exp Neurol. 2016; 75:673–688. [PubMed: 27283328]
43. Moubarik C, Guillet B, Youssef B, et al. Transplanted late outgrowth endothelial progenitor cells as cell therapy product for stroke. Stem Cell Rev. 2011; 7:208–220. [PubMed: 20526754]
44. Fan Y, Shen F, Frenzel T, et al. Endothelial progenitor cell transplantation improves long-term stroke outcome in mice. Ann Neurol. 2010; 67:488–497. [PubMed: 20437584]
45. Ishikawa H, Tajiri N, Shinozuka K, et al. Vasculogenesis in experimental stroke after human cerebral endothelial cell transplantation. Stroke. 2013; 44:3473–3481. [PubMed: 24130140]
46. De Bock M, Van Haver V, Vandenbroucke RE, et al. Into rather unexplored terrain-transcellular transport across the blood-brain barrier. Glia. 2016; 64:1097–1123. [PubMed: 26852907]
47. Doll DN, Hu H, Sun J, et al. Mitochondrial crisis in cerebrovascular endothelial cells opens the blood-brain barrier. Stroke. 2015; 46:1681–1689. [PubMed: 25922503]
48. Tajiri N, Acosta S, Glover LE, et al. Intravenous grafts of amniotic fluid-derived stem cells induce endogenous cell proliferation and attenuate behavioral deficits in ischemic stroke rats. Plos ONE. 2012; 7:e43779. [PubMed: 22912905]
49. Matsukawa N, Yasuhara T, Hara K, et al. Therapeutic targets and limits of minocycline neuroprotection in experimental ischemic stroke. BMC Neurosci. 2009; 10:126. [PubMed: 19807907]
50. Yasuhara T, Matsukawa N, Hara K, et al. Notch-induced rat and human bone marrow stromal cell grafts reduce ischemic cell loss and ameliorate behavioral deficits in chronic stroke animals. Stem Cells Dev. 2009; 18:1501–1514. [PubMed: 19301956]
51. Borlongan CV, Kaneko Y, Maki M, et al. Menstrual blood cells display stem cell-like phenotypic markers and exert neuroprotection following transplantation in experimental stroke. Stem Cells Dev. 2010; 19:439–452. [PubMed: 19860544]
52. Rosell A, Arai K, Lok J, et al. Interleukin-1beta augments angiogenic responses of murine endothelial progenitor cells in vitro. J Cereb Blood Flow Metab. 2009; 29:933–943. [PubMed: 19240740]
53. Hayakawa K, Pham L-DD, Katusic ZS, et al. Astrocytic high-mobility group box 1 promotes endothelial progenitor cell-mediated neurovascular remodeling during stroke recovery. Proc Natl Acad Sci USA. 2012; 109:7505–7510. [PubMed: 22529378]
54. Koh S-H, Liang AC, Takahashi Y, et al. Differential Effects of Isoxazole-9 on Neural Stem/Progenitor Cells, Oligodendrocyte Precursor Cells, and Endothelial Progenitor Cells. Plos ONE. 2015; 10:e0138724. [PubMed: 26407349]
55. Lee HJ, Kim KS, Kim EJ, et al. Brain transplantation of immortalized human neural stem cells promotes functional recovery in mouse intracerebral hemorrhage stroke model. Stem Cells. 2007; 25:1204–1212. [PubMed: 17218400]
56. Jeong S-W, Chu K, Jung K-H, et al. Human neural stem cell transplantation promotes functional recovery in rats with experimental intracerebral hemorrhage. Stroke. 2003; 34:2258–2263. [PubMed: 12881607]

57. Acosta SA, Tajiri N, Hoover J, et al. Intravenous bone marrow stem cell grafts preferentially migrate to spleen and abrogate chronic inflammation in stroke. Stroke. 2015; 46:2616–2627. [PubMed: 26219646]
58. Yu S, Tajiri N, Franzese N, et al. Stem cell-like dog placenta cells afford neuroprotection against ischemic stroke model via heat shock protein upregulation. Plos ONE. 2013; 8:e76329. [PubMed: 24086730]
59. Paxinos, G., Watson, C. The Rat Brain in Stereotaxic Coordinates (Deluxe Edition), Fourth Edition. 4th. Academic Press; 1998.
60. Tremblay M-E, Riad M, Majewska A. Preparation of mouse brain tissue for immunoelectron microscopy. J Vis Exp. 2010; (41):e2021.
61. Hanker JS. Osmiophilic reagents in electronmicroscopic histocytochemistry. Prog Histochem Cytochem. 1979; 12:1–85. [PubMed: 92799]
62. Graham RC, Karnovsky MJ. The early stages of absorption of injected horseradish peroxidase in the proximal tubules of mouse kidney: ultrastructural cytochemistry by a new technique. J Histochem Cytochem. 1966; 14:291–302. [PubMed: 5962951]
63. Voet, D., Voet, JG., Pratt, CW. Fundamentals of biochemistry: life at the molecular level. New York: Wiley; 2006.
64. McBride HM, Neuspiel M, Wasiak S. Mitochondria: more than just a powerhouse. Curr Biol. 2006; 16:R551–R560. [PubMed: 16860735]
65. Hajnóczky G, Csordás G, Das S, et al. Mitochondrial calcium signalling and cell death: approaches for assessing the role of mitochondrial Ca2+ uptake in apoptosis. Cell Calcium. 2006; 40:553–560. [PubMed: 17074387]
66. Li X, Fang P, Mai J, et al. Targeting mitochondrial reactive oxygen species as novel therapy for inflammatory diseases and cancers. J Hematol Oncol. 2013; 6:19. [PubMed: 23442817]
67. Green DR. Apoptotic pathways: the roads to ruin. Cell. 1998; 94:695–698. [PubMed: 9753316]
68. Tajiri N, Borlongan CV, Kaneko Y. Cyclosporine A Treatment Abrogates Ischemia-Induced Neuronal Cell Death by Preserving Mitochondrial Integrity through Upregulation of the Parkinson's Disease-Associated Protein DJ-1. CNS Neurosci Ther. 2016; 22:602–610. [PubMed: 27247192]
69. Kaneko Y, Tajiri N, Shojo H, et al. Oxygen-glucose-deprived rat primary neural cells exhibit DJ-1 translocation into healthy mitochondria: a potent stroke therapeutic target. CNS Neurosci Ther. 2014; 20:275–281. [PubMed: 24382215]
70. Kaneko Y, Shojo H, Burns J, et al. DJ-1 ameliorates ischemic cell death in vitro possibly via mitochondrial pathway. Neurobiol Dis. 2014; 62:56–61. [PubMed: 24060818]
71. Li J, Ma X, Yu W, et al. Reperfusion promotes mitochondrial dysfunction following focal cerebral ischemia in rats. Plos ONE. 2012; 7:e46498. [PubMed: 23029539]
72. Wang DB, Uo T, Kinoshita C, et al. Bax interacting factor-1 promotes survival and mitochondrial elongation in neurons. J Neurosci. 2014; 34:2674–2683. [PubMed: 24523556]
73. Tao J, Liu W, Shang G, et al. MiR-207/352 regulate lysosomal-associated membrane proteins and enzymes following ischemic stroke. Neuroscience. 2015; 305:1–14. [PubMed: 26232047]
74. Li Q, Zhang T, Wang J, et al. Rapamycin attenuates mitochondrial dysfunction via activation of mitophagy in experimental ischemic stroke. Biochem Biophys Res Commun. 2014; 444:182–188. [PubMed: 24440703]
75. Ito U, Kuroiwa T, Hanyu S, et al. Temporal profile of experimental ischemic edema after threshold amount of insult to induce infarction--ultrastructure, gravimetry and Evans' blue extravasation. Acta Neurochir Suppl. 2003; 86:131–135. [PubMed: 14753420]
76. Adembri C, Venturi L, Tani A, et al. Neuroprotective effects of propofol in models of cerebral ischemia: inhibition of mitochondrial swelling as a possible mechanism. Anesthesiology. 2006; 104:80–89. [PubMed: 16394694]
77. Stanika RI, Pivovarova NB, Brantner CA, et al. Coupling diverse routes of calcium entry to mitochondrial dysfunction and glutamate excitotoxicity. Proc Natl Acad Sci USA. 2009; 106:9854–9859. [PubMed: 19482936]
78. Ito U, Hakamata Y, Kawakami E, et al. Degeneration of astrocytic processes and their mitochondria in cerebral cortical regions peripheral to the cortical infarction: heterogeneity of their

disintegration is closely associated with disseminated selective neuronal necrosis and maturation of injury. Stroke. 2009; 40:2173–2181. [PubMed: 19359621]

79. Liu H, Zhang X, Du Y, et al. Leonurine protects brain injury by increased activities of UCP4, SOD, CAT and Bcl-2, decreased levels of MDA and Bax, and ameliorated ultrastructure of mitochondria in experimental stroke. Brain Res. 2012; 1474:73–81. [PubMed: 22842526]
80. Rapoport SI, Ohno K, Pettigrew KD. Drug entry into the brain. Brain Res. 1979; 172:354–359. [PubMed: 466480]
81. Pardridge WM. Brain drug delivery and blood-Brain barrier transport. Drug Delivery. 1993; 1:83–101.
82. Weiss N, Miller F, Cazaubon S, et al. The blood-brain barrier in brain homeostasis and neurological diseases. Biochim Biophys Acta. 2009; 1788:842–857. [PubMed: 19061857]
83. Stewart PA. Endothelial vesicles in the blood-brain barrier: are they related to permeability? Cell Mol Neurobiol. 2000; 20:149–163. [PubMed: 10696507]
84. Engelhardt B, Sorokin L. The blood-brain and the blood-cerebrospinal fluid barriers: function and dysfunction. Semin Immunopathol. 2009; 31:497–511. [PubMed: 19779720]
85. Chaudhuri JD. Blood brain barrier and infection. Med Sci Monit. 2000; 6:1213–1222. [PubMed: 11208482]
86. Abbott NJ, Patabendige AAK, Dolman DEM, et al. Structure and function of the blood-brain barrier. Neurobiol Dis. 2010; 37:13–25. [PubMed: 19664713]
87. Minshall RD, Tiruppathi C, Vogel SM, et al. Vesicle formation and trafficking in endothelial cells and regulation of endothelial barrier function. Histochem Cell Biol. 2002; 117:105–112. [PubMed: 11935286]
88. Claudio L, Kress Y, Norton WT, et al. Increased vesicular transport and decreased mitochondrial content in blood-brain barrier endothelial cells during experimental autoimmune encephalomyelitis. Am J Pathol. 1989; 135:1157–1168. [PubMed: 2596575]
89. Emr, S., Kelly, R., Pelham, H., et al. Molecular Biology of the Cell. 4th. New York: Garland Science; 2002. Chapter 13: Intracellular Vesicular Traffic.
90. Takeshita Y, Ransohoff RM. Inflammatory cell trafficking across the blood-brain barrier: chemokine regulation and in vitro models. Immunol Rev. 2012; 248:228–239. [PubMed: 22725965]
91. Borlongan CV, Glover LE, Tajiri N, et al. The great migration of bone marrow-derived stem cells toward the ischemic brain: therapeutic implications for stroke and other neurological disorders. Prog Neurobiol. 2011; 95:213–228. [PubMed: 21903148]
92. Borlongan CV. Bone marrow stem cell mobilization in stroke: a “bonehead” may be good after all! Leukemia. 2011; 25:1674–1686. [PubMed: 21727900]
93. Urbich C, Dimmeler S. Endothelial progenitor cells: characterization and role in vascular biology. Circ Res. 2004; 95:343–353. [PubMed: 15321944]
94. Tongers J, Roncalli JG, Losordo DW. Role of endothelial progenitor cells during ischemia-induced vasculogenesis and collateral formation. Microvasc Res. 2010; 79:200–206. [PubMed: 20144623]
95. Kirton JP, Xu Q. Endothelial precursors in vascular repair. Microvasc Res. 2010; 79:193–199. [PubMed: 20184904]
96. Kaneko Y, Tajiri N, Shinozuka K, et al. Cell therapy for stroke: emphasis on optimizing safety and efficacy profile of endothelial progenitor cells. Curr Pharm Des. 2012; 18:3731–3734. [PubMed: 22574986]
97. Zhao Y-H, Yuan B, Chen J, et al. Endothelial progenitor cells: therapeutic perspective for ischemic stroke. CNS Neurosci Ther. 2013; 19:67–75. [PubMed: 23230897]
98. Bai Y-Y, Peng X-G, Wang L-S, et al. Bone Marrow Endothelial Progenitor Cell Transplantation After Ischemic Stroke: An Investigation Into Its Possible Mechanism. CNS Neurosci Ther. 2015; 21:877–886. [PubMed: 26384586]

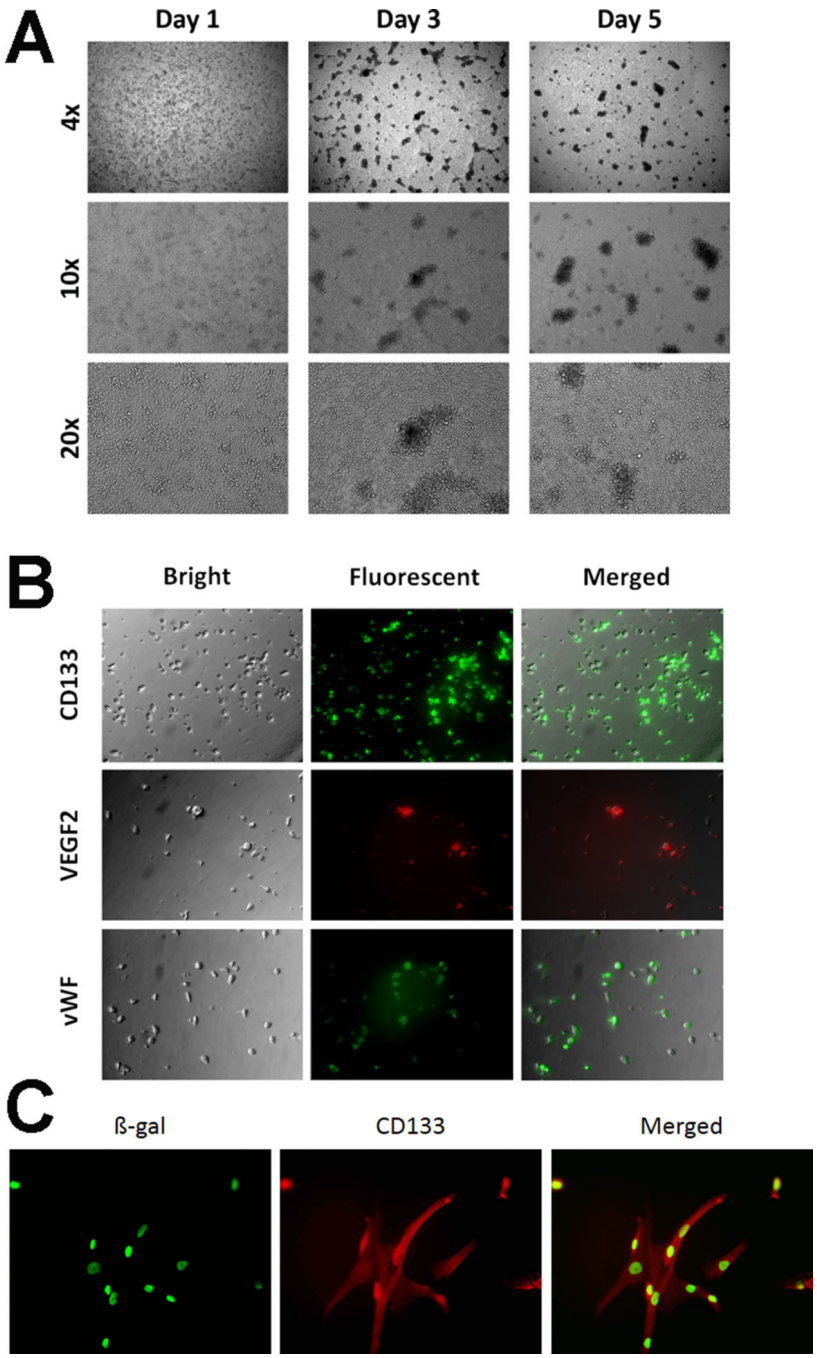

Figure 1. Immunocytochemical characteristics of isolated hBMEPCs and cells labeled with β-galactosidase (β-gal) *in vitro*

(**A**) After Day 1 in culture, isolated MNCs from human bone marrow already began to attach onto collagen I-coated plates and were characterized by conglobate cell bodies with clear cytoplasm. Subsequent culture at Day 3 revealed cells exhibiting spindle-shape morphology with some cell-to-cell network appearance and formation of small colonies. At Days 5–7 in culture, more cells continued to form networks and larger colonies with about 80% of these colonies reaching confluence with the characteristic cobblestone-like monolayer. The phase-

contrast images obtained at 4X, 10X, 20X magnifications. (**B**) Early EPCs were phenotyped at Day 5 in culture using direct fluorescent immunostaining with surface-antigen expression of markers such as CD133, VEGF-2 (KDR), and vWF, and revealed 86%, 76%, and 82% positivity for each marker, respectively. Magnification at 10X. (**C**) As a surrogate marker for subsequent transplantation of hBMEPCs, cells were labeled with β-gal, and such labeling produced >90% β-gal-positive hBMEPCs (green). Magnification at 20X.

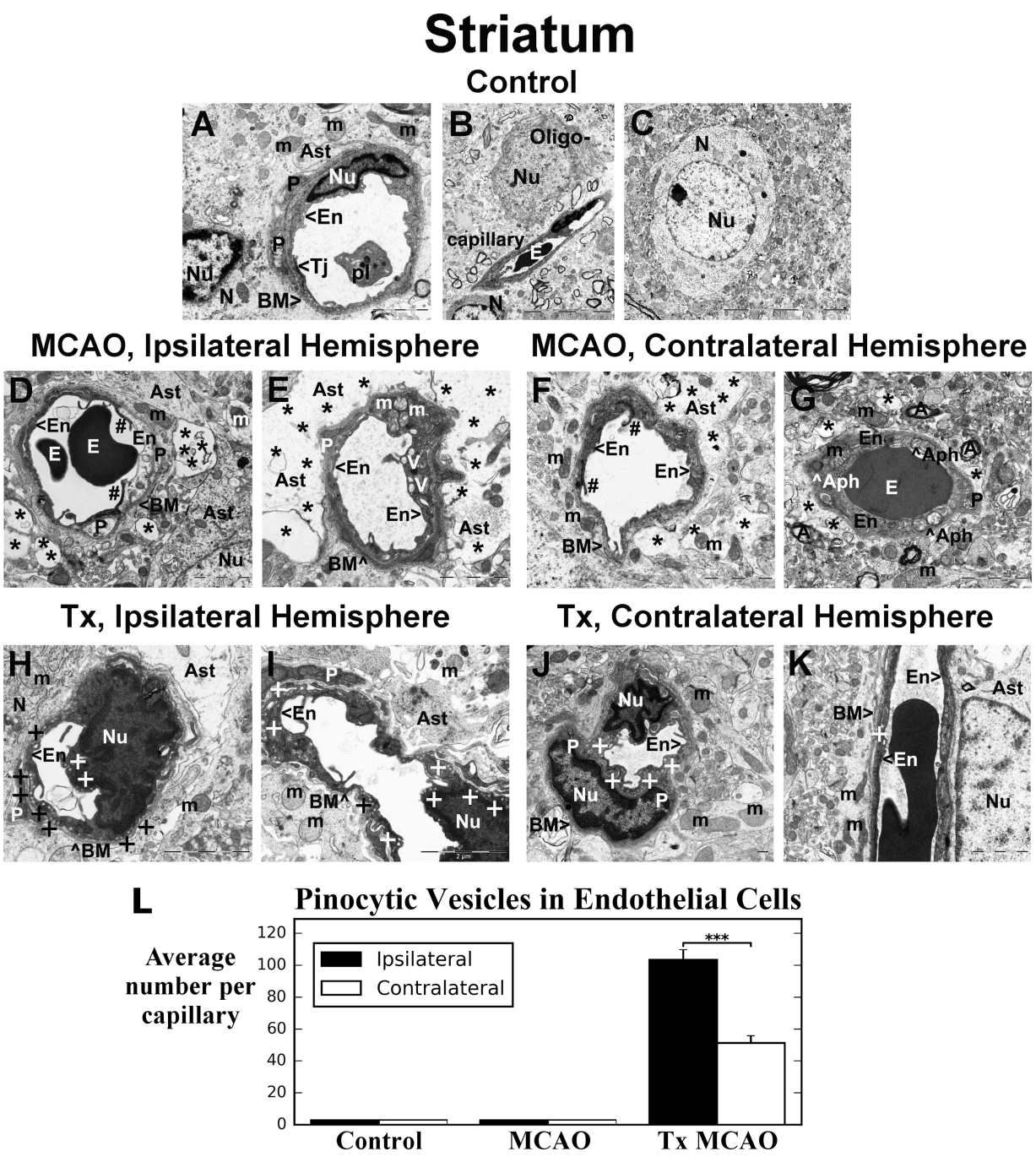

Figure 2. Electron microscopic examination of microvasculature in the striatum of tMCAO rat after hBMEPC transplant

Control rat (**A, B, C**) striatum showed normal ultrastructural capillary morphology. In hemisphere ipsilateral to tMCAO, necrotic EC with condensed cytoplasm (**D**) and ECs with numerous large vacuoles and swollen mitochondria (**E**) were determined. Degenerated pericyte is apparent. Large extracellular edema separated astrocyte end-feet from capillary. In contralateral striatum, capillaries contained necrotic (**F**) or swollen EC with enlarged vacuolated mitochondria and autophagosomes (**G**). Some edema surrounded capillaries. (**H,**

I) Five days after hBMEPC transplant, numerous striatum capillaries ipsilateral to tMCAO insult demonstrated normal morphology. ECs displayed many pinocytic vesicles, indicating pinocytosis. No perivascular edema was noted. Healthy pericytes, neurons, and astrocytes were observed. (**J, K**) In contralateral striatum, vesicles in ECs were also visible, although fewer compared to ipsilateral hemisphere capillaries. No perivascular edema was determined. There was normal ultrastructure of capillaries and surrounding astrocytes. The number of animals per group is n=4. **En** - endothelial cell, **BM** - basement membrane, **Tj** – tight junction, **Ast** – astrocyte, **E** – erythrocyte, **pl** – platelets, **m** – mitochondrion, **N** - neuron, **Oligo**- - oligodendrocyte, **P** – pericyte, **A** – axon, **Nu** – nucleus, **Aph** - autophagosome. Asterisks in **D–G** indicate extracellular edema; + in **H–K** indicates vesicle. Scale bar in A, D-K is 2 μm; in B, C is 10 μm.

(**L**) Significantly ($p < 0.001$) more pinocytic vesicles in capillary ECs in ipsilateral vs. contralateral hemisphere were determined in striatum of tMCAO rat after hBMEPC transplant. No pinocytic vesicles were detected in non-treated tMCAO or control rats.

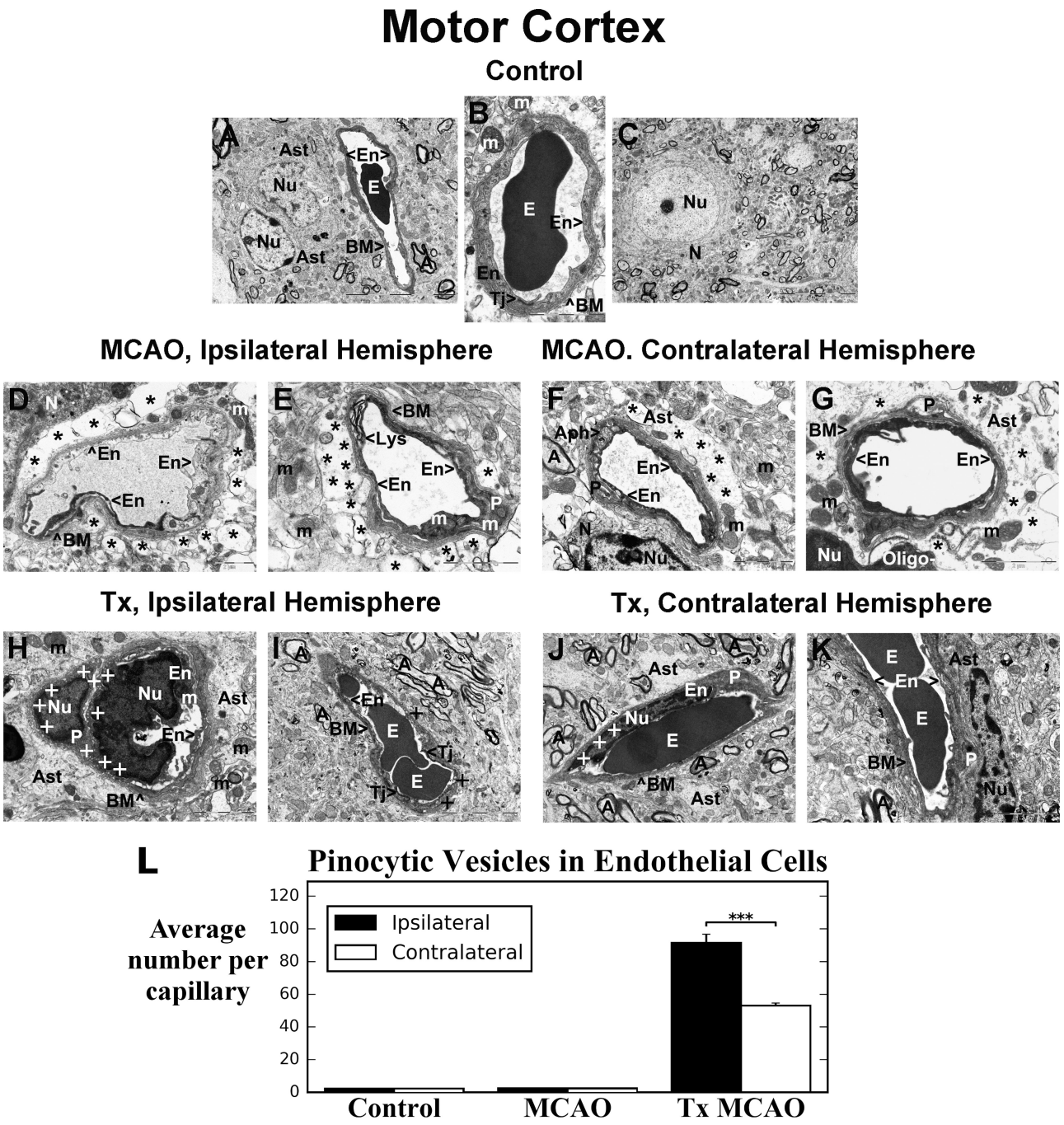

Figure 3. Electron microscopic examination of microvasculature in the motor cortex of tMCAO rat after hBMEPC transplant

Similarly to striatum, capillaries in control motor cortex showed typical ultrastructural morphology (**A, B, C**). In hemisphere ipsilateral to tMCAO, necrotic EC was adjacent to swollen EC (**D**). Swollen mitochondria in EC and in degenerated pericyte were visible (**E**). Extensive perivascular edema was seen (**D, E**). In contralateral hemisphere, capillaries showed necrotic ECs (**F, G**) with adjacent swollen EC containing autophagosomes (**F**). Perivascular edema and degenerated pericytes were noted. After hBMEPC transplant,

capillaries ipsilateral to tMCAO demonstrated normal ultrastructure of ECs, pericytes, and astrocyte processes (**H, I**). Similarly to striatum, cortical capillary ECs displayed many pinocytic vesicles. Importantly, pericyte also showed vesicles (**H**). No perivascular edema was observed. (**J, K**) Contralateral hemisphere capillaries had fewer EC vesicles. Perivascular edema was also lacking. There was normal ultrastructure of capillaries, astrocyte, and pericytes. The number of animals per group is n=4. (See Figure 2 for explanation of abbreviations.) Scale bar in B, D, F, G, H, J, K is 2 μm; in E is 1 μm; in I is 5 μm; in A, C is 10 μm.

(**L**) Significantly ($p < 0.001$) more pinocytic vesicles were detected in capillary ECs in ipsilateral vs. contralateral hemisphere in motor cortex of cell-treated tMCAO rats. There were no pinocytic vesicles within capillaries in non-treated tMCAO or control rats.

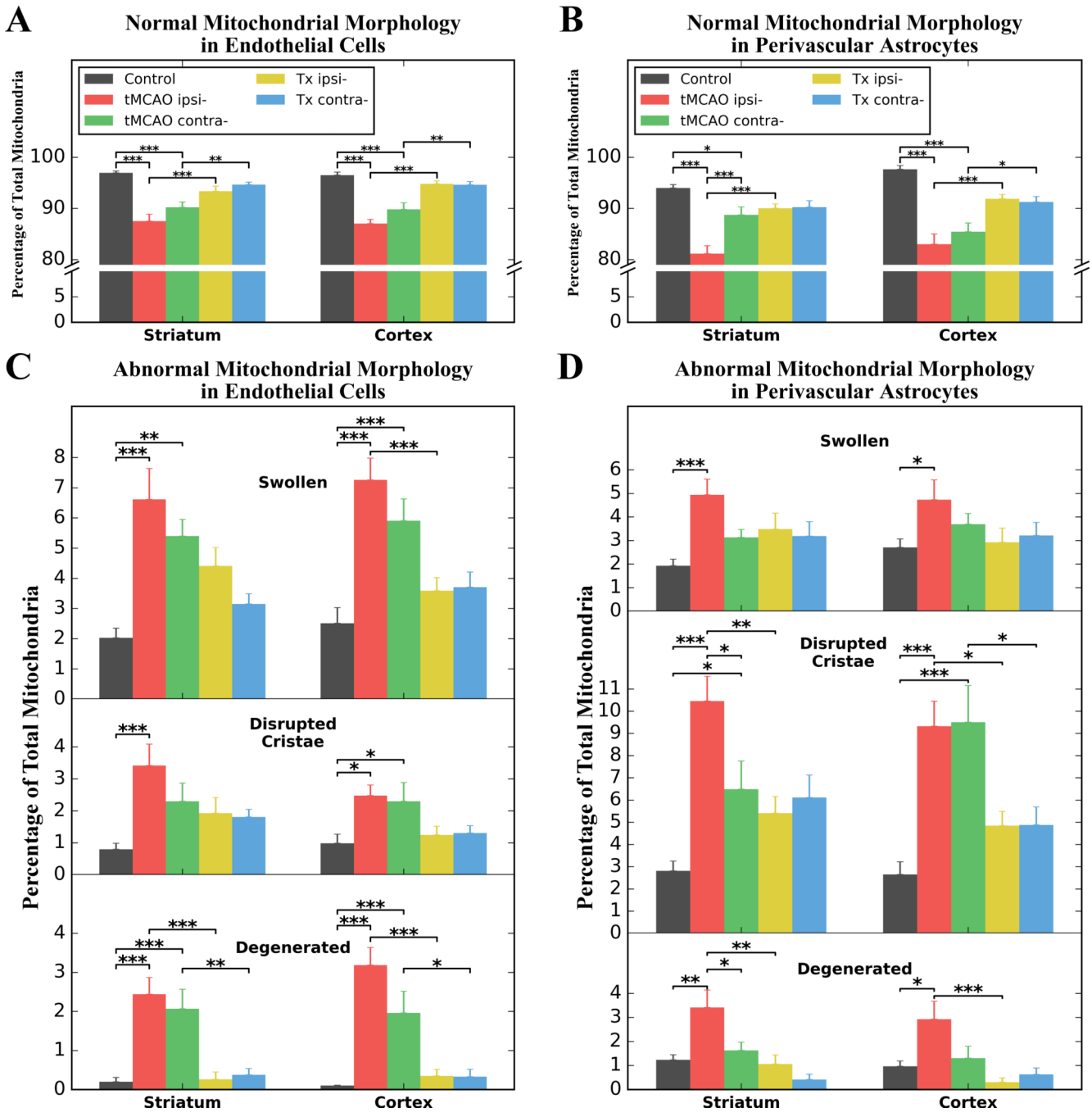

Figure 4. Quantitative morphological characteristics of mitochondria in endothelial cells and perivascular astrocytes

(**A**) Significant reductions of mitochondria with normal morphology within ECs in both hemispheres in striatum and motor cortex were determined in tMCAO rats 7 days after insult. In hBMEPC-treated tMCAO rats, significant increase of normal mitochondria within ECs was detected in striatum and cortex of both brain hemispheres vs. non-treated tMCAO rats. (**B**) Significant decreases of normal mitochondria were also noted in perivascular astrocytes of tMCAO rats in striatal/cortical areas of both hemispheres. Significantly greater

percentages of normal mitochondria were noted in ipsilateral hemisphere of striatum/motor cortex of cell-treated vs. non-treated tMCAO rats. In contralateral hemisphere, significant differences between hBMEPC-treated and non-treated tMCAO rats were detected only in cortical areas. Analysis showed (**C**) significantly higher percentages of abnormal mitochondria in ipsilateral ECs in striatum/motor cortex of non-treated tMCAO rats vs. controls. In contralateral hemisphere, significantly increased abnormal mitochondria were also noted in tMCAO rats. After hBMEPC treatment, abnormal mitochondria in ECs were reduced. Degenerated mitochondria were almost undetectable in ECs of treated animals compared to tMCAO rats. (**D**) In perivascular astrocytes, higher percentages of abnormal mitochondria in striatum/motor cortex of both hemispheres were found in tMCAO rats. These abnormal mitochondria were reduced in striatum and cortex of both hemispheres in hBMEPC-treated tMCAO rats. Degenerated mitochondria were significantly decreased in ipsilateral striatum and cortex in cell-treated vs. stroke animals. *$p < 0.05$, **$p < 0.01$, ***$p < 0.001$.